Surface Chemistry Hot Paper

International Edition: DOI: 10.1002/anie.201502999
German Edition: DOI: 10.1002/ange.201502999

Size-Dependent Ligand Layer Dynamics in Semiconductor Nanocrystals Probed by Anisotropy Measurements**

*Ido Hadar, Tsafrir Abir, Shira Halivni, Adam Faust, and Uri Banin**

Abstract: *Colloidal semiconductor nanocrystals (NC) have reached a high level of synthetic control allowing the tuning of their properties, and their use in various applications. However, the surface of NCs and in particular their size-dependent capping organic ligand behavior, which play an important role in the NC synthesis, dispersibility, and optoelectronic properties, is still not well understood. We study the size-dependent properties of the ligand shell on the surface of NCs, by embedding surface bound dyes as a probe within the ligand shell. The reorientation times for these dyes show a linear dependence on the NC surface curvature indicating size-dependent change in viscosity, which is related to a change in the density of the ligand layer because of the geometry of the surface, a unique feature of NCs. Understanding the properties of the ligand shell will allow rational design of the surface to achieve the desired properties, providing an additional important knob for tuning their functionality.*

Colloidal semiconductor nanocrystals (NCs) are promising building blocks for various applications, as already demonstrated in their use for fluorescent biological tagging,[1,2] and as chromophores in back light units of liquid-crystal displays as well as advanced research in additional devices including solid-state lighting, solar cells, photodetectors, and field-effect transistors.[3–8] This is mainly due to the ability to modify the physical and chemical properties of the semiconductor material through bottom-up approaches by controlling the particles size and shape in the nanometer scale.[9–11] The inorganic NC surface is typically coated by an organic ligand layer, making NCs a unique inorganic–organic hybrid chemical system. Considering the inherent high surface-to-volume ratios of such NCs, the ligand layer is of paramount importance in the NC synthesis and in affecting the chemical and physical properties of the particles.[12] In the NC synthesis, the ligand layer plays a central role in size- and shape-controlled growth.[13] Moreover, the ligand layer makes possible the use of different solvents and matrices for the NC dispersion, and ligand exchange is a common approach to manipulate the NC compatibility within different environments.[14] The surface ligands also play a role in surface passivation by saturating dangling orbitals of the NC surface atoms, and hence avoiding irreversible chemical reactivity at the surface (chemical passivation), as well as playing some role in the passivation of electronic surface trap states (physical passivation).

Several methods have been employed to study the ligands on the surface of NCs. These are based on identification of the ligands themselves, or alternatively, on probing the surface-ligand-dependent properties of the NCs.[15] NMR spectroscopy has emerged as a major technique to study the properties of organic ligands on the surface of NCs, due to its ability to trace specific ligands in their natural environment by a non-destructive procedure, and the capability to quantitatively distinguish between free and bound ligands.[16] Using NMR spectroscopy, researchers have been able to study important aspects of the ligand shell such as the surface coverage, binding mechanism, surface stoichiometry, and ligand exchange schemes.[17–21] A major limitation of NMR spectroscopy is that a high concentration of NCs is needed in order to gain sufficient signal-to-noise ratios, concentrations that are much higher than the typical concentration used for other analysis techniques and for most applications. This makes the use of NMR spectroscopy more prohibitive, and in certain cases may even lead to misleading conclusions. In addition, there is need for in situ approaches for the study of the surface effects which can allow for fast and efficient probing of low NC concentrations. Herein we study the size-dependent dynamic properties of the nanocrystal ligand shell using fluorescence anisotropy measurements of probe dye molecules bound to the nanocrystal surface. A similar approach was used previously to study self-assembled monolayers on bulk surfaces.[22] In this approach, organic dye molecules were attached directly to the surface of NCs[23–25] and their reorientation dynamics were probed by time-resolved fluorescence anisotropy spectroscopy.[26] The dye molecules are embedded inside the ligand shell and adapt the dynamic properties of the ligands. Their reorientation times are hence sensitive to the size-dependent effective viscosity of the ligand layer. The approach is applicable to low concentrations of nanocrystals in situ, and benefits also from the advantages of other optical probes including high sensitivity, potentially down to the single nanocrystals level, with use in diverse environments, at different temperatures, and under various conditions.

To probe the size-dependent ligand dynamics in this manner, we synthesized four samples of CdSe/CdS core/shell quantum dots (QDs), with radii ranging between 1.3 to 2.4 nm, capped with octadecylamine ligands (Figure 1a; see

[*] I. Hadar, T. Abir, S. Halivni, A. Faust, Prof. U. Banin
Institute of Chemistry and the Center for Nanoscience and Nanotechnology, The Hebrew University of Jerusalem
Jerusalem, 91904 (Israel)
E-mail: uri.banin@mail.huji.ac.il

[**] The research leading to these results has received funding from the Israel Science Foundation—ISF, grant number 811/13. U.B. thanks the Alfred & Erica Larisch memorial chair.

Supporting information for this article including the synthesis, experimental setup, and data analysis is available on the WWW under http://dx.doi.org/10.1002/anie.201502999.

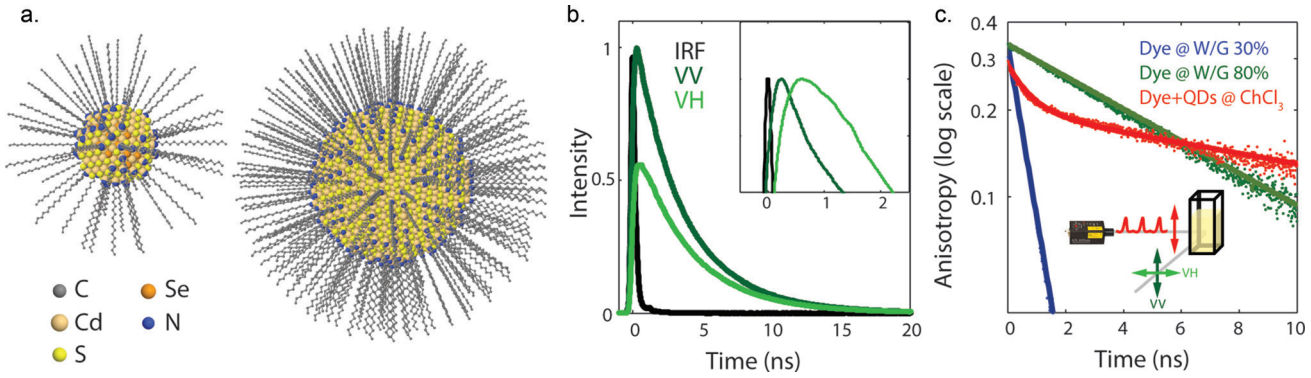

Figure 1. a) Illustration of CdSe/CdS core/shell QDs (radius of 1.3 and 2.4 nm) and of the surface ligand shell. b) Time-resolved photoselection measurements of Atto647N dye in water/glycerol mixture. Initially the intensity is higher at the parallel direction (VV) than the horizontal direction (VH), and as time evolves the reorientation dynamics takes place reducing the anisotropy. The reorientation kinetics is further manifested in the inset, showing a delay in the emission maxima of the perpendicular direction (the intensity in the inset is normalized for clarity). From these measurements the time-resolved anisotropy is calculated. c) Time-resolved anisotropy (dots), and fits (solid lines), of dye in low (blue) and high (green) viscosity medium, and of the dye in QDs–dye conjugates sample (red). While for the dye alone, the anisotropy follows a single exponential decay, for the QDs–dye conjugates a more complex, bi-exponential decay is observed, which reflects the dual population of free and bound dyes within this sample.

the Supporting Information). We use Atto 647N dye with an amine linker group for surface binding to the QDs, as the probe molecules. In principle, the linker amine group attaches to positive binding sites—the Cd atoms on the surface of the QD, similar to the binding of the native amine ligands to the QD surface. In order to achieve effective conjugation of the dye molecules, excess native ligands were removed from the QD solutions by successive precipitation and dissolution steps. The cleaned QDs were dispersed in chloroform at concentration of about 100 nM and mixed with the dye solution (in chloroform) at molar ratio of approximately five dye molecules per QD. According to a previous study,[24] such treatment will yield the attachment of a few dye molecules to each QD, relative to a few hundreds or thousands of ligands, hence the dye molecules are not expected to change the dynamic properties of the ligand shell.

Upon conjugation, the samples were measured in a time-resolved photoselection scheme (see the Supporting Information for full description). Briefly the solution is excited by a vertically polarized pulsed laser (635 nm, 100 ps pulse), which preferably excites the dye molecules that are aligned with their absorption transition dipole moment along the vertical direction. Following excitation, the emission intensities in the parallel–vertical (I_{VV}) and perpendicular–horizontal (I_{VH}) polarizations are measured and the time-resolved anisotropy, $r_{(t)}$, is calculated according to Equation (1).

$$r_{(t)} = \frac{I_{VV(t)} - I_{VH(t)}}{I_{VV(t)} + 2 \cdot I_{VH(t)}} \tag{1}$$

An example for such measurement is presented in Figure 1 b, showing the time-resolved emission decays at parallel and perpendicular polarizations. The emission intensity is corrected for any polarization response of the measurement system. Immediately after the excitation the excited dyes emit preferentially in the parallel direction (emission and absorption dipole moments are parallel). With time, the dye molecules reorient and thus the anisotropy returns to zero value. If the typical reorientation time (θ) is in the order of the natural decay time of the emitter (τ), the time-resolved anisotropy will decay exponentially with time according to Equation (2),

$$r_{(t)} = r_0 \cdot \exp\left(-\frac{t}{\theta}\right) \tag{2}$$

where r_0 is the anisotropy of the emitter in the absence of reorientation effects (at time zero, see the Supporting Information for full derivation).

The reorientation dynamics of free dye molecules in water/glycerol mixtures were measured as reference (Figure 1 c). The expected single exponential decay was observed, and the reorientation time was found to scale with the viscosity of the medium (η). The additional factors that determine the reorientation time are related to the volume and shape of the dye (V,f, respectively), interactions with the medium (C), and the thermal energy (k_bT) [Eq. (3)].

$$\theta = \frac{\eta V f C}{k_b T} \tag{3}$$

For the QD–dye samples, the results of the reorientation dynamics differ substantially (red curve in Figure 1 c). A bi-exponential decay of the anisotropy was observed. This is a clear indication that the dye molecules in the solution are divided to two populations—free dye molecules and QD–dye conjugates, respectively showing fast and slow reorientation times. We verified that for each specific sample the ratio between the fast and slow components (or free and bound dye molecules, respectively), reaches equilibrium (usually within few minutes after adding the dye molecules to the solution), and remains stable throughout the measurements.

The reorientation time constants for the various sizes of QDs were extracted by fitting the anisotropy curves to a bi-exponential decay function, the relative fraction of each population can be derived from the amplitude of each

component and it can be used to evaluate the ratio between free and bound dye. The reorientation time of the slow component is significantly longer compared to the free dye in chloroform. Moreover, it strongly depends on the QD size and becomes shorter as the size is decreased, from 21 ns for the NCs with a 2.4 nm radius, to 11 ns for the NCs with a 1.3 nm radius (Figure 2a,b). Furthermore, changing the measurement temperature between 15 to 45 °C, which significantly changes the viscosity of the medium (chloroform), has hardly any effect on the reorientation time of the bound dye molecules (Figure 2b). This is a direct indication that the measured slow component of the reorientation time for the bound dyes, is related to an effective viscosity of the ligand shell, and not to tumbling of the entire QD which is expected to be much longer, and expected to depend on the solvent viscosity. Moreover, the relative independence of reorientation times on temperature indicates that for these samples and in this temperature range, the ligands do not exhibit a dramatic change in their physical properties such as a phase transfer. This result emphasizes the ability of time-resolved anisotropy to directly probe the dynamic properties of the ligands, in contrast to previous studies that relied on indirect measurements of certain ligand-dependent properties of the NC such as the photoluminescence[27] or chemical reactivity towards metal growth.[28]

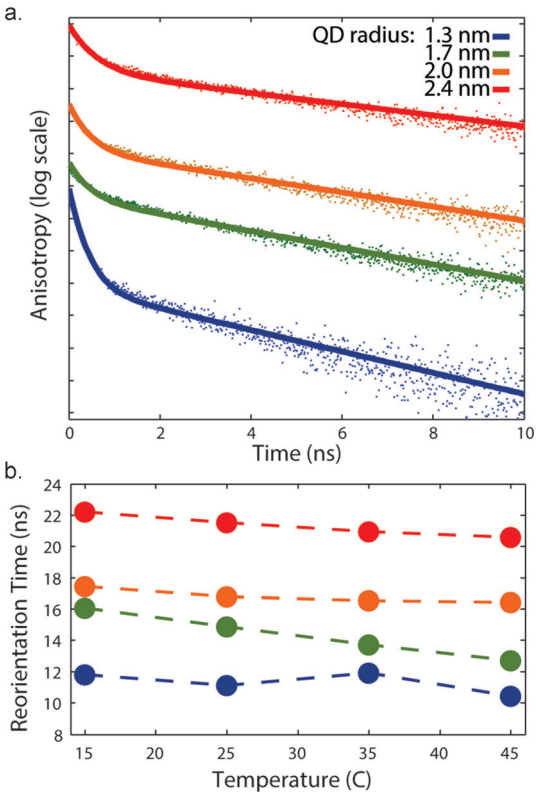

Figure 2. a) Time-resolved anisotropy measurements (dots), and fits to bi-exponential decay (solid lines), of the QDs–dye conjugates for QDs samples of different radii. The changes in the reorientation times for the slow component with QD radius can be seen by the change in the slope of the long decay component of the anisotropy. Data is vertically shifted for clarity. b) Reorientation times of the dye molecules attached to the surface of the various samples of QDs (slow component of the bi-exponential decay), as function of temperature, showing only moderate change in this temperature range (dashed lines are a guide for the eye).

To gain further insight regarding the effect of NC size and of its surface curvature on the dynamic properties of the ligand shell, the reorientation times of the bound dyes are plotted versus the curvature of the QDs, which for a sphere is the reciprocal of the radius, in Figure 3. It is clearly seen that the reorientation time of the bound dyes becomes longer as the curvature decreases, and an inverse linear relation between the curvature and the reorientation time, is observed. Fitting to linear function provides an expected reorientation for a flat surface (curvature equals zero), of about 32 ns.

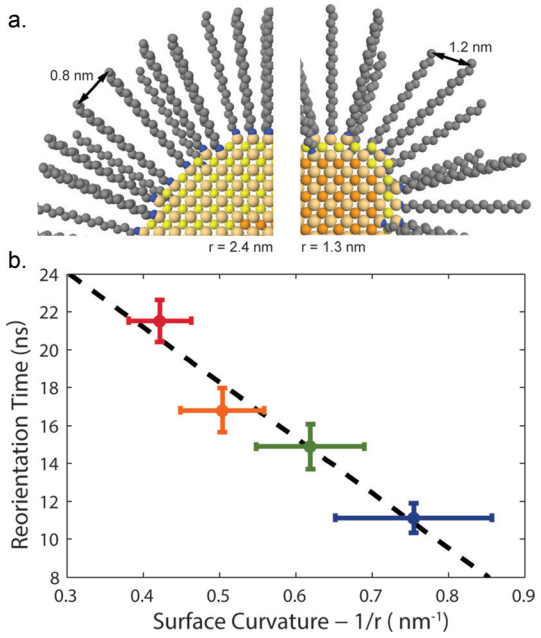

Figure 3. a) Cross section of QDs and their capping ligand shell. From this illustration the change in the density of the ligand shell, manifested by the larger distances between ligands at the outer shell for the smaller QD can be clearly discerned. b) Reorientation times versus the QD surface curvature showing a linear correlation. From fitting this data, a reorientation time of about 32 ns is expected for infinite flat surface.

We next discuss the origin for the systematic change in the reorientation times upon varying the NC radius. The main factors considered relate to those affecting the ability of the ligands, and hence the probe molecule, to reorient more freely within the ligand monolayer. The two major factors are first, the density of the binding of the ligands—that is, ligand surface coverage effect, and second, the effective density of the ligand shell constraining movements within the monolayer. For organic ligands bound to a surface, two types of motions are allowed: rotational movement of the ligands around the bond axis and bending of the ligand with respect to

the surface. Both modes are expected to be slowed down when the density of the binding increases, which results in an increase of the density of the ligand shell. For QDs, however, certain deviation from this trend is expected. While the surface binding density of the ligands is assumed to be similar for all QDs (or even slightly higher for smaller QDs), the actual density of the ligand shell farther from the surface is reduced because of the curvature, as was also demonstrated for gold QDs covered with oligonucleotides.[29–31] For the smaller QDs this effect is stronger, and thus as the size of the QD decreases the ligands can move more freely. This can be represented by the effective viscosity of the ligand layer, which is lowered as shown uniquely by our study. This phenomenon is distinctive to nanoscale surfaces that shows curvature which is in the order of magnitude of the width of the ligand shell.

In order to estimate the change in density with QD radius, we assume a constant binding density of ligands at the surface of the QDs (four ligands per square-nanometer)[15,16] and calculate the surface density at the outer shell of the ligand monolayer (about 2 nm from the surface), for the different sizes of the QDs. The change in the density is illustrated in Figure 3a, presenting a close up view of the surfaces for two QDs, 2.4 nm and 1.3 nm in radius. The change in the ligand density along with the changes in the reorientation times for the QDs with the different radii are summarized in Table 1.

Table 1: Summary of size-dependent reorientation times and ligand density in the different QD samples.

QD Radius [nm]	Curvature [nm^{-1}]	Reorientation coefficient [ns]	Density at the outer shell [nm^{-2}]	Area per ligand at the outer shell [nm^2]
1.3 ± 0.2	0.8 ± 0.1	11 ± 1	0.6 ± 0.1	1.6 ± 0.1
1.6 ± 0.2	0.6 ± 0.1	15 ± 1	0.8 ± 0.1	1.3 ± 0.1
2.0 ± 0.2	0.5 ± 0.1	17 ± 1	1.0 ± 0.1	1.0 ± 0.1
2.4 ± 0.3	0.4 ± 0.1	21 ± 1	1.2 ± 0.1	0.8 ± 0.1

As can be seen from the results of this illustrative model, indeed the available space for reorientation for each ligand is increased for the smaller QDs. For the larger QDs the constraints for movement are higher, limiting the capability of each ligand to move freely and hence increasing the effective viscosity of the ligand shell which is indicated by the slower reorientation dynamics of the probe dye molecules.

In summary, we have used for the first time anisotropy measurements of a probe dye molecule bound to the NC surface, to investigate the NC ligand dynamics. The bi-exponential decay directly allowed us to separate the bound from free ligand components. An inverse linear correlation of the reorientation times with the NC surface curvature was found, and assigned to the change of density of the ligand shell, indicating geometrical dependence of the effective viscosity of this layer. The fluorescence anisotropy is therefore a useful in situ probe for the surface ligand layer behavior, and offers a unique view on the size-dependent dynamic properties of the ligands in the nanocrystals.

Keywords: fluorescence spectroscopy · nanocrystals · nanotechnology · polarized spectroscopy · surface chemistry

How to cite: *Angew. Chem. Int. Ed.* **2015**, *54*, 12463–12467
Angew. Chem. **2015**, *127*, 12640–12644

[1] M. Bruchez, Jr., M. Moronne, P. Gin, S. Weiss, A. P. Alivisatos, *Science* **1998**, *281*, 2013–2016.
[2] W. C. Chan, S. Nie, *Science* **1998**, *281*, 2016–2018.
[3] Y. Shirasaki, G. J. Supran, M. G. Bawendi, V. Bulović, *Nat. Photonics* **2012**, *7*, 13–23.
[4] T.-H. Kim, D.-Y. Chung, J. Ku, I. Song, S. Sul, D.-H. Kim, K.-S. Cho, B. L. Choi, J. M. Kim, S. Hwang, et al., *Nat. Commun.* **2013**, *4*, 2637.
[5] T.-H. Kim, K.-S. Cho, E. K. Lee, S. J. Lee, J. Chae, J. W. Kim, D. H. Kim, J.-Y. Kwon, G. Amaratunga, S. Y. Lee, B. L. Choi, Y. Kuk, J. M. Kim, K. Kim, *Nat. Photonics* **2011**, *5*, 176–182.
[6] L. J. Diguna, Q. Shen, J. Kobayashi, T. Toyoda, *Appl. Phys. Lett.* **2007**, *91*, 023116.
[7] J. H. Bang, P. V. Kamat, *ACS Nano* **2009**, *3*, 1467–1476.
[8] A. Salant, M. Shalom, I. Hod, A. Faust, A. Zaban, U. Banin, *ACS Nano* **2010**, *4*, 5962–5968.
[9] A. P. Alivisatos, *J. Phys. Chem.* **1996**, *100*, 13226–13239.
[10] C. B. Murray, D. J. Norris, M. G. Bawendi, *J. Am. Chem. Soc.* **1993**, *115*, 8706–8715.
[11] D. V. Talapin, J.-S. Lee, M. V. Kovalenko, E. V. Shevchenko, *Chem. Rev.* **2010**, *110*, 389–458.
[12] J. Owen, *Science* **2015**, *347*, 615–616.
[13] X. Peng, L. Manna, W. Yang, J. Wickham, E. Scher, A. Kadavanich, A. Alivisatos, *Nature* **2000**, *404*, 59–61.
[14] A. Dong, X. Ye, J. Chen, Y. Kang, T. Gordon, J. M. Kikkawa, C. B. Murray, *J. Am. Chem. Soc.* **2011**, *133*, 998–1006.
[15] A. J. Morris-Cohen, M. Malicki, M. D. Peterson, J. W. J. Slavin, E. A. Weiss, *Chem. Mater.* **2013**, *25*, 1155–1165.
[16] Z. Hens, J. C. Martins, *Chem. Mater.* **2013**, *25*, 1211–1221.
[17] J. R. Sachleben, E. W. Wooten, L. Emsley, A. Pines, V. L. Colvin, A. P. Alivisatos, *Chem. Phys. Lett.* **1992**, *198*, 431–436.
[18] J. S. Owen, J. Park, P.-E. Trudeau, A. P. Alivisatos, *J. Am. Chem. Soc.* **2008**, *130*, 12279–12281.
[19] N. C. Anderson, M. P. Hendricks, J. J. Choi, J. S. Owen, *J. Am. Chem. Soc.* **2013**, *135*, 18536–18548.
[20] B. Fritzinger, I. Moreels, P. Lommens, R. Koole, Z. Hens, J. C. Martins, *J. Am. Chem. Soc.* **2009**, *131*, 3024–3032.
[21] A. Hassinen, I. Moreels, C. de Mello Donegá, J. C. Martins, Z. Hens, *J. Phys. Chem. Lett.* **2010**, *1*, 2577–2581.
[22] D. S. Karpovich, G. J. Blanchard, *Langmuir* **1996**, *12*, 5522–5524.
[23] I. Potapova, R. Mruk, C. Hübner, R. Zentel, T. Basché, A. Mews, *Angew. Chem. Int. Ed.* **2005**, *44*, 2437–2440; *Angew. Chem.* **2005**, *117*, 2490–2493.
[24] I. Hadar, S. Halivni, N. Even-Dar, A. Faust, U. Banin, *J. Phys. Chem. C* **2015**, *119*, 3849–3856.
[25] X. Li, V. M. Nichols, D. Zhou, C. Lim, G. S. H. Pau, C. J. Bardeen, M. L. Tang, G. Shu, H. Pau, J. Bardeen, *Nano Lett.* **2014**, *14*, 3382–3387.
[26] J. R. Lakowicz, *Principles of Fluorescence Spectroscopy*, Springer, Singapore, **2006**.
[27] S. F. Wuister, A. van Houselt, C. de Mello Donegá, D. Vanmaekelbergh, A. Meijerink, *Angew. Chem. Int. Ed.* **2004**, *43*, 3029–3033; *Angew. Chem.* **2004**, *116*, 3091–3095.

[28] G. Menagen, J. E. Macdonald, Y. Shemesh, I. Popov, U. Banin, *J. Am. Chem. Soc.* **2009**, *131*, 17406 – 17411.
[29] W. J. Parak, T. Pellegrino, C. M. Micheel, D. Gerion, S. C. Williams, A. P. Alivisatos, *Nano Lett.* **2003**, *3*, 33 – 36.
[30] S. Park, K. A. Brown, K. Hamad-Schifferli, *Nano Lett.* **2004**, *4*, 1925 – 1929.
[31] T. Pellegrino, R. A. Sperling, A. P. Alivisatos, W. J. Parak, *J. Biomed. Biotechnol.* **2007**, *2007*, 26796.

Received: April 1, 2015
Revised: April 20, 2015
Published online: May 26, 2015

